

Simultaneous Visual Data Completion and Denoising based on Tensor Rank and Total Variation Minimization and its Primal-dual Splitting Algorithm

Tatsuya Yokota Hidekata Hontani
Nagoya Institute of Technology
Gokiso, Showa, Nagoya, 466-8555, Japan
{t.yokota, hontani}@nitech.ac.jp

Abstract

Tensor completion has attracted attention because of its promising ability and generality. However, there are few studies on noisy scenarios which directly solve an optimization problem consisting of a “noise inequality constraint”. In this paper, we propose a new tensor completion and denoising model including tensor total variation and tensor nuclear norm minimization with a range of values and noise inequalities. Furthermore, we developed its solution algorithm based on a primal-dual splitting method, which is computationally efficient as compared to tensor decomposition based non-convex optimization. Lastly, extensive experiments demonstrated the advantages of the proposed method for visual data retrieval such as for color images, movies, and 3D-volumetric data.

1. Introduction

Completion is a technique of filling missing elements of incomplete data using the values of reference (available) elements and the structural assumptions (priors) of data. When the reference and missing elements are independent, *e.g.*, white noise, completion is impossible. However, most real-world data have a few redundant properties that can be used for completion, such as symmetry, repetition, and sparsity. For example, the frequency-domain of natural images is typically considerably sparse, and this property leads to an efficient compression ratio in a JPEG encoder [31]. Moreover, data obtained using multi-spectral imaging or microphone arrays can frequently be represented by linear combinations of a few patterns, which allows for efficient data analysis, such as low-rank matrix/tensor decompositions [25, 12]. Structural assumptions must be used in completion to obtain good performance, and assumptions about the structure of data affect the results of completion.

In recent years, low-rank priors have gained importance in matrix and tensor completion problems [6, 23] and sig-

nal separation [21, 4]. A promising application of low-rank based completion is a recommender system, which automatically recommends appropriate products for customers based on purchase history. As there is no noise in this type of data, standard noiseless matrix and tensor completion frameworks can be applied [3, 7, 24, 18, 8, 23, 20]. In this case, nuclear norm minimization is regarded as the standard approach because strict rank minimization is NP-hard [11], and a nuclear norm relaxes the NP-hard problem to a convex optimization problem [26].

Visual data retrieval is another application of low-rank based completion. However, it typically requires matrix and tensor completion frameworks in a noisy scenario [17, 5, 15], and using only low-rank priors may not be sufficient. In this study, we address the challenging problem of simultaneous matrix and tensor completion and denoising. Low-rank based matrix completion in a noisy scenario, which minimizes a matrix nuclear norm under a noise inequality constraint, has been discussed in [5]. However, this algorithm involves solving convex optimization problems multiple times to tune a hyperparameter. The following two critical issues exist: (1) Solving an optimization problem, which includes a noise inequality constraint, using convex optimization only once. (2) Developing a robust model of matrix/tensor completion in a noisy scenario.

To resolve issue (1), in this study, we propose a primal-dual splitting (PDS) algorithm [9] for problems consisting of proximable functions and constraints. For this purpose, we derive that the proximal mapping of a noise inequality constraint, which is not trivial, can be obtained using analytical calculation. Furthermore, to improve the robustness against noise (issue (2)), we introduce total variation (TV) regularization for a tensor while considering tensor nuclear norm minimization. The proposed flexible model can include low-rank exact/inexact matrix/tensor completion with/without TV regularization. In practice, there are several types of visual data such as low-rank oriented, low-TV oriented, and intermediate. As the proposed model can adjust the weights of low-rank and low-TV priors, various

types of data can be retrieved flexibly.

The remainder of this paper is organized as follows: In Section 2, prior studies on matrix and tensor completion methods are reviewed. In Sections 3 and 4, we propose a new model for tensor completion based on low rank and TV, and its optimization algorithm using a PDS approach. In Section 5, we demonstrate the advantages of the proposed method over selected state-of-the-art methods using color images, movies, and 3D-volumetric images. Lastly, we state the conclusions in Section 6.

1.1. Notations

The notations used in this paper follow several rules. A vector, a matrix, and a tensor are denoted by a bold lowercase letter, $\mathbf{a} \in \mathbb{R}^I$, a bold uppercase letter, $\mathbf{B} \in \mathbb{R}^{I \times J}$, and a bold calligraphic letter, $\mathcal{C} \in \mathbb{R}^{J_1 \times J_2 \times \dots \times J_N}$, respectively. An N -th-order tensor, $\mathcal{X} \in \mathbb{R}^{I_1 \times I_2 \times \dots \times I_N}$, can be transformed into a vector and N matrix forms, which are denoted using the same character, $\mathbf{x} \in \mathbb{R}^{\prod_{n=1}^N I_n}$ and $\mathbf{X}_{(n)} \in \mathbb{R}^{I_n \times \prod_{k \neq n} I_k}$ for $n \in \{1, 2, \dots, N\}$, respectively. An (i_1, i_2, \dots, i_N) -element of \mathcal{X} is denoted by x_{i_1, i_2, \dots, i_N} or $[\mathcal{X}]_{i_1, i_2, \dots, i_N}$. Operator \otimes represents the Hadamard product, defined as $[\mathcal{X} \otimes \mathcal{Z}]_{i_1, i_2, \dots, i_N} = x_{i_1, i_2, \dots, i_N} z_{i_1, i_2, \dots, i_N}$.

2. Review of prior works in matrix and tensor completion

We consider a general matrix/tensor completion problem as follows:

$$\underset{\mathcal{X}}{\text{minimize}} f(\mathcal{X}), \text{ s.t. } \|P_\Omega(\mathcal{X} - \mathcal{T})\|_F^2 \leq \delta, \quad (1)$$

where \mathcal{T} and $\mathcal{X} \in \mathbb{R}^{I_1 \times I_2 \times \dots \times I_N}$ are the input and output N -th order tensors, respectively, a cost function, $f(\cdot) : \mathbb{R}^{I_1 \times I_2 \times \dots \times I_N} \rightarrow \mathbb{R}$, is used to evaluate structural assumptions, $P_\Omega(\mathcal{Z}) := \mathcal{Q} \otimes \mathcal{Z}$ with $\mathcal{Q} \in \{0, 1\}^{I_1 \times I_2 \times \dots \times I_N}$ is an index tensor that represents the missing and available elements of \mathcal{T} as 0 and 1, respectively. A support set, Ω , is defined as $\Omega := \{(i_1, i_2, \dots, i_N) \mid q_{i_1, i_2, \dots, i_N} = 1\}$. The value of δ depends on the noise level of the observed elements in \mathcal{T} , and on missing ratio $\rho := 1 - \frac{|\Omega|}{\prod_{n=1}^N I_n}$.

As an inequality constraint is relatively difficult to address, its Lagrange-like optimization problem is commonly used, given by

$$\underset{\mathcal{X}}{\text{minimize}} f(\mathcal{X}) + \frac{\mu}{2} \|P_\Omega(\mathcal{X} - \mathcal{T})\|_F^2, \quad (2)$$

where μ is a trade-off parameter between a prior and an error term.

Problems (1) and (2) are linked by δ and μ . Figure 1 shows the relationship between δ and μ in tensor completion. In hyperparameter selection, δ can be selected from $[0, \sigma^2|\Omega|]$ or a narrower range considered in [5] if noise variance σ^2 is known; in contrast, μ is typically selected from

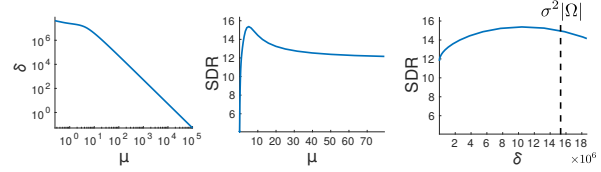


Figure 1. Examples of relationships of μ vs δ (left), μ vs signal-to-distortion ratio (SDR) (center), and δ vs SDR (right).

$(0, \infty)$. Based on this, we claim that Problem (1) is more suitable than Problem (2) for hyperparameter selection.

2.1. Matrix completion models

First, we consider a matrix completion problem, which is a case of $N = 2$ in (1). When $\delta = 0$, Problem (1) is referred to as ‘exact’ matrix completion.

In [5], a case where the cost function is given by a nuclear norm has been discussed, where the nuclear norm of matrix $\mathbf{Z} \in \mathbb{R}^{I \times J}$ is defined by $\|\mathbf{Z}\|_* := \sum_{i=1}^{\min(I, J)} \sigma_i(\mathbf{Z})$, and $\sigma_i(\mathbf{Z})$ is the i -th largest singular value of \mathbf{Z} . To solve Problem (1) with the nuclear norm, an algorithm has been proposed, which requires solving

$$\mathbf{X}_\mu^* = \underset{\mathbf{X}}{\text{argmin}} \|\mathbf{X}\|_* + \frac{\mu}{2} \|P_\Omega(\mathbf{X} - \mathbf{T})\|_F^2, \quad (3)$$

multiple times to determine an appropriate value of $\mu > 0$ such that $\|P_\Omega(\mathbf{X}_\mu^* - \mathbf{T})\|_F^2 = \delta$. As iterative calculations of singular value decomposition are required to solve Problem (3) [24], the algorithm is computationally expensive. We refer to this algorithm as low-rank matrix completion with noise (LRMCn).

There are several studies about applications of image deblurring, denoising, and interpolation [27, 30, 13], where a cost function is given by TV. The standard TV for matrix $\mathbf{Z} \in \mathbb{R}^{I \times J}$ is defined by

$$\|\mathbf{Z}\|_{\text{TV}} := \sum_{i, j} \sqrt{(\nabla_1 z_{i, j})^2 + (\nabla_2 z_{i, j})^2}, \quad (4)$$

where an n -th mode partial differential operator is defined by $\nabla_n z_{i_1, i_2, \dots, i_N} := z_{i_1, \dots, (i_n+1), \dots, i_N} - z_{i_1, \dots, i_n, \dots, i_N}$.

Problem (2) with the nuclear norm and TV is discussed in [28], in which it was proposed to minimize the nuclear norm using singular value thresholding and TV using gradient descent, alternately. However, using standard gradient-based optimization is not appropriate because the nuclear norm and TV are not differentiable functions. An alternative efficient optimization approach referred to as ‘proximal splitting’ is gaining attention [9, 1]. We discuss using this approach for Problem (1) in this paper.

2.2. Tensor completion models

When $N \geq 3$ in (1), it is not a simple extension of matrix completion because of special properties of tensors. For

example, there are two types of ranks in tensors, i.e., the canonical polyadic (CP) rank and Tucker rank [19]. As the CP rank has several difficult properties, low Tucker-rank based completion is relatively well studied.

In [22, 23], a case of exact tensor completion, which is Problem (1) with $\delta = 0$, where the cost function is given by a tensor nuclear norm has been discussed, in which the tensor nuclear norm, $f_{\text{LR}}(\mathcal{X})$, is defined by

$$f_{\text{LR}}(\mathcal{X}) := \sum_{n=1}^N \lambda_n \|\mathbf{X}_{(n)}\|_*, \quad (5)$$

where $\lambda_n \geq 0$ ($\forall n$) represents the weight parameters for individual tensor modes, and $\mathbf{X}_{(n)} \in \mathbb{R}^{I_n \times \prod_{k \neq n} I_k}$ is the n -th mode unfolded matrix of tensor \mathcal{X} . The alternating direction method of multipliers (ADMM) [2] has been employed. Furthermore, its noisy scenario has been discussed in [10], which is formulated as Problem (2) with the tensor nuclear norm. We refer to this method as low n -rank tensor completion (LNRTC).

In [14], a case of Problem (2), in which the cost function is given by generalized TV (GTV) has been discussed, where GTV is defined by the sum of the generalized matrix TV of individual mode-unfolded matrices of a tensor as

$$f_{\text{GTV}}(\mathcal{X}) := \sum_{n=1}^N w_n \|\mathbf{X}_{(n)}\|_{\text{GTV}}, \quad (6)$$

where $w_n \geq 0$ ($\forall n$) represents the weight parameters for individual tensor modes, and $\|\mathbf{Z}\|_{\text{GTV}}$ for matrix $\mathbf{Z} \in \mathbb{R}^{I \times J}$ is a GTV-norm, which is defined by

$$\|\mathbf{Z}\|_{\text{GTV}} := \sum_{i,j} \sqrt{\sum_{\theta \in \Theta} \tau_{\theta} (\tilde{\nabla}_{\theta} z_{i,j})^2}, \quad (7)$$

where $\tau_{\theta} \geq 0$ represents weight parameters, $\tilde{\nabla}_{\theta}$ is the differential operator for direction θ , for example, $\tilde{\nabla}_0 z_{i,j} = z_{(i+1),j} - z_{i,j}$, $\tilde{\nabla}_{45} z_{i,j} = z_{(i+1),(j+1)} - z_{i,j}$, $\tilde{\nabla}_{90} z_{i,j} = z_{i,(j+1)} - z_{i,j}$, and $\tilde{\nabla}_{135} z_{i,j} = z_{(i-1),(j+1)} - z_{i,j}$. This convex optimization problem is solved using the ADMM in [14]. We typically consider $\Theta = \{0, 90\}$ for standard matrix TV (4). In contrast, $\Theta = \{0, 45, 90, 135\}$ is considered for GTV. When we consider $\Theta = \{0\}$ and $\tau_0 = 1$ for all n in GTV, it is given by $f_{\text{GTV}}(\mathcal{Z}) = \sum_{n=1}^N w_n \sum_{i_1, i_2, \dots, i_N} |\nabla_n z_{i_1, i_2, \dots, i_N}| = \sum_{i_1, i_2, \dots, i_N} \sum_{n=1}^N w_n |\nabla_n z_{i_1, i_2, \dots, i_N}|$. In this case, GTV is anisotropic with respect to N modes in the tensors, which leads to corruption of diagonal edges.

Note that we can consider a more simple, straightforward, and isotropic tensorial extension of matrix TV, which is defined by

$$f_{\text{TV}}(\mathcal{Z}) := \sum_{i_1, i_2, \dots, i_N} \sqrt{\sum_{n=1}^N w_n (\nabla_n z_{i_1, i_2, \dots, i_N})^2}. \quad (8)$$

Instead of GTV, we consider this TV in this paper.

3. Proposed model

In this section, we propose a new model for tensor completion and denoising using a tensor nuclear norm and TV simultaneously. The proposed optimization problem is given by

$$\begin{aligned} & \underset{\mathcal{X}}{\text{minimize}} \quad \alpha f_{\text{TV}}(\mathcal{X}) + \beta f_{\text{LR}}(\mathcal{X}), \\ & \text{s.t.} \quad v_{\min} \leq \mathcal{X} \leq v_{\max}, \\ & \quad \quad \|P_{\Omega}(\mathcal{T} - \mathcal{X})\|_F^2 \leq \delta, \end{aligned} \quad (9)$$

where $0 \leq \alpha \leq 1$ and $\beta := 1 - \alpha$ are the weight parameters between the TV and nuclear norm terms, and the first constraint in (9) imposes all values of the output tensor to be included in a range, $[v_{\min}, v_{\max}]$. The first and second constraints are convex and the indicator functions are given by

$$i_{\mathcal{D}}(\mathcal{X}) := \begin{cases} 0 & v_{\min} \leq \mathcal{X} \leq v_{\max} \\ \infty & \text{otherwise} \end{cases}, \quad (10)$$

$$i_{\delta}(\mathcal{X}) := \begin{cases} 0 & \|P_{\Omega}(\mathcal{T} - \mathcal{X})\|_F^2 \leq \delta \\ \infty & \text{otherwise} \end{cases}. \quad (11)$$

Using $i_{\mathcal{D}}(\mathcal{X})$ and $i_{\delta}(\mathcal{X})$, tensor completion problem (9) can be rewritten as the minimization of $\alpha f_{\text{TV}}(\mathcal{X}) + \beta f_{\text{LR}}(\mathcal{X}) + i_{\mathcal{D}}(\mathcal{X}) + i_{\delta}(\mathcal{X})$. As these four functions are not differentiable, traditional gradient-based optimization algorithms, e.g., the Newton method, cannot be applied. In Section 4, we introduce and apply an efficient approach, referred to as PDS, to solve proposed optimization problem (9).

3.1. Characterization of the proposed model

In this section, we explain the relationship between the proposed model and prior works introduced in Section 2. There are three characterizations of the proposed model.

First, when $N = 2$, $\alpha = 0$, $\beta = 1$, $\lambda = [1, 0]^T$, $v_{\min} = -\infty$, and $v_{\max} = \infty$, the proposed model can be characterized as LRMCn [5]. In contrast with LRMCn, which solves several convex optimization problems to tune μ , the proposed method can obtain its solution by solving only one convex optimization problem, and provides its tensorial extension.

Second, when $\alpha = 0$, $\beta = 1$, $v_{\min} = -\infty$, and $v_{\max} = \infty$, the proposed method can be characterized as LNRTC [10]. In contrast with LNRTC, which employs the ADMM for solving a type of Problem (2), the proposed method employs the PDS algorithm for solving a type of Problem (1).

Third, when $\alpha = 1$, $\beta = 0$, $v_{\min} = -\infty$, and $v_{\max} = \infty$, the proposed model can be characterized as an isotropic version of GTV [14]. In contrast with GTV, in which a problem

is solved using the ADMM, which requires matrix inversion through the fast Fourier transform (FFT) and inverse FFT, the proposed method does not need to consider matrix inversion. Furthermore, the proposed method tunes the value of δ instead of μ .

Additionally, our model differs from a recent work proposed in [16] because it applies some constrained fixed-rank matrix factorization models into individual mode-matricization of a same tensor in noiseless scenario. The problem is non-convex and it is not designed for a noise reduction model.

4. Optimization

4.1. Primal-dual splitting algorithm

The PDS [9] algorithm is a framework used to split an optimization problem including non-differentiable functions into several sub-optimization processes using proximal operators. The proximal operator of a function, $g(\cdot)$, is defined as

$$\text{prox}_g(\mathcal{Z}) := \underset{\mathcal{X}}{\text{argmin}} g(\mathcal{X}) + \frac{1}{2} \|\mathcal{X} - \mathcal{Z}\|_F^2, \quad (12)$$

where \mathcal{Z} and \mathcal{X} are arbitrary variables. When the proximal operator of $g(\cdot)$ can be calculated analytically, $g(\cdot)$ is referred to as a ‘proximable function’. First, we introduce the general framework of the PDS algorithm for convex optimization. We consider the following optimization problem:

$$\begin{aligned} \underset{\mathbf{x}}{\text{minimize}} \quad & f(\mathbf{x}) + \sum_{j=1}^J h_j(\mathbf{y}_j), \\ \text{s.t.} \quad & \mathbf{y}_j = \mathbf{L}_j \mathbf{x}, \end{aligned} \quad (13)$$

where $f(\cdot)$ and $h_j(\cdot)$ are convex proximable functions, \mathbf{x} and \mathbf{y}_j are the primal and dual variables, respectively, and \mathbf{L}_j represents linear operators. Optimization problem (13) is convex and can be solved using the following PDS algorithm:

$$\mathbf{x}^{k+1} = \text{prox}_{\gamma_1 f} \left[\mathbf{x}^k - \gamma_1 \sum_{j=1}^J \mathbf{L}_j^T \mathbf{y}_j^k \right]; \quad (14)$$

$$\tilde{\mathbf{y}}_j^{k+1} = \mathbf{y}_j^k + \gamma_2 (2\mathbf{x}^{k+1} - \mathbf{x}^k); \quad (\forall j) \quad (15)$$

$$\mathbf{y}_j^{k+1} = \tilde{\mathbf{y}}_j^{k+1} - \gamma_2 \text{prox}_{\frac{1}{\gamma_2} h_j} \left[\frac{1}{\gamma_2} \tilde{\mathbf{y}}_j^{k+1} \right]; \quad (\forall j) \quad (16)$$

where $\gamma_1 > 0$ and $\gamma_2 > 0$ are step-size parameters for the primal and dual steps, respectively.

4.2. Proposed algorithm

In this section, we apply the PDS algorithm to the proposed optimization problem. Introducing dual variables

$\mathbf{U} \in \mathbb{R}^{I_1 \times I_2 \times \dots \times I_N}$, $\mathbf{Y} = [\mathbf{y}_1, \mathbf{y}_2, \dots, \mathbf{y}_N] \in \mathbb{R}^{\prod_{n=1}^N I_n \times N}$, and $\{\mathcal{Z}^{(n)} \in \mathbb{R}^{I_1 \times I_2 \times \dots \times I_N}\}_{n=1}^N$, Problem (9) can be rewritten as

$$\begin{aligned} \underset{\mathbf{x}}{\text{minimize}} \quad & i_\delta(\mathcal{X}) + i_D(\mathbf{U}) \\ & + \alpha \|\mathbf{Y}\|_{2,1} + \beta \sum_{n=1}^N \lambda_n \|\mathcal{Z}^{(n)}\|_*, \quad (17) \\ \text{s.t.} \quad & \mathbf{U} = \mathcal{X}, \mathbf{y}_n = \sqrt{w_n} \mathbf{D}_n \mathbf{x} \quad (\forall n), \\ & \mathcal{Z}^{(n)} = \mathcal{X} \quad (\forall n), \end{aligned}$$

where $\mathbf{x} \in \mathbb{R}^{\prod_{n=1}^N I_n}$ is the vectorized form of \mathcal{X} and \mathbf{D}_n is the linear differential operator of the n -th mode of the tensor. $\|\cdot\|_{2,1}$ is the $l_{2,1}$ -norm of the matrix, defined as $\|\mathbf{Z}\|_{2,1} := \sum_{i=1}^I \sqrt{\sum_{j=1}^J z_{ij}^2}$ for matrix $\mathbf{Z} \in \mathbb{R}^{I \times J}$. Algorithm 1 can be derived using the PDS framework in Problem (17). We refer to this algorithm as the ‘low-rank and TV (LRTV)–PDS’ algorithm.

Note that the $l_{2,1}$ -norm, the nuclear norm, i_D , and i_δ are proximable functions whose calculations are given by

$$\text{prox}_{\gamma \|\cdot\|_{2,1}}(\mathbf{Z}) = \mathbf{Z} \otimes [\mathbf{s}, \dots, \mathbf{s}], \quad (18)$$

$$\text{prox}_{\gamma \|\cdot\|_*}(\mathbf{Z}) = \mathbf{U} \max(\mathbf{\Sigma} - \gamma, 0) \mathbf{V}^T, \quad (19)$$

$$\text{prox}_{i_D}(\mathcal{Z}) = \max(\min(\mathcal{Z}, v_{\max}), v_{\min}), \quad (20)$$

$$\text{prox}_{i_\delta}(\mathcal{Z}) = \tilde{\mathcal{Q}} \otimes \mathcal{T} + (1 - \tilde{\mathcal{Q}}) \otimes \mathcal{Z}, \quad (21)$$

where $\mathbf{s} = [s_1, \dots, s_I]^T \in \mathbb{R}^I$ with $s_i = \max\left(1 - \frac{\gamma}{\|\mathbf{z}_i\|_2}, 0\right)$ for $\mathbf{Z} = [\mathbf{z}_1, \mathbf{z}_2, \dots, \mathbf{z}_I]^T \in \mathbb{R}^{I \times J}$, ($\mathbf{U}, \mathbf{\Sigma}, \mathbf{V}$) are the left, center-diagonal, and right matrices, respectively, of the singular value decomposition of \mathbf{Z} , and $\tilde{\mathcal{Q}} = \max\left(0, 1 - \frac{\sqrt{\delta}}{\|\mathcal{Q} \otimes (\mathcal{Z} - \mathcal{T})\|_F}\right) \mathcal{Q}$. Proximal operators (18), (19), and (20) are well known; however, (21) is not. Thus, we prove (21) in Section 4.2.1.

4.2.1 Proof of (21)

To prove (21), we consider the following problem:

$$\min_{\mathcal{X}} \frac{1}{2} \|\mathcal{Z} - \mathcal{X}\|_F^2 \text{ s.t. } \|\mathcal{Q} \otimes (\mathcal{T} - \mathcal{X})\|_F^2 \leq \delta. \quad (22)$$

For elements $q_{i_1, i_2, \dots, i_N} = 0$, the optimization problem can be expressed as the minimization of $(z_{i_1, i_2, \dots, i_N} - x_{i_1, i_2, \dots, i_N})^2$. Thus, we obtain

$$x_{i_1, i_2, \dots, i_N}^* = z_{i_1, i_2, \dots, i_N} \quad (q_{i_1, i_2, \dots, i_N} = 0). \quad (23)$$

Eq. (21) satisfies (23).

For elements $q_{i_1, i_2, \dots, i_N} = 1$, the optimization problem is given as

$$\min_{\mathbf{x}_q} \frac{1}{2} \|\mathbf{z}_q - \mathbf{x}_q\|_2^2 \text{ s.t. } \|\mathbf{t}_q - \mathbf{x}_q\|_2^2 \leq \delta, \quad (24)$$

Algorithm 1 LRTV-PDS algorithm

- 1: **input** : $\mathcal{T}, \mathcal{Q}, \delta, v_{\min}, v_{\max}, \alpha, \mathbf{w}, \beta, \boldsymbol{\lambda}, \gamma_1, \gamma_2$;
 - 2: **initialize** : $\mathcal{X}^0, \mathcal{U}^0, \mathcal{Y}^0, \mathcal{Z}^{(n)0} (\forall n), k = 0$;
 - 3: **repeat**
 - 4: $\mathbf{v} \leftarrow \mathbf{u}^k + \sum_{n=1}^N \mathbf{z}^{(n)k} + \sum_{n=1}^N \sqrt{w_n} \mathbf{D}_n^T \mathbf{y}_n^k$;
 - 5: $\mathbf{x}^{k+1} = \text{prox}_{i_\delta} [\mathbf{x}^k - \gamma_1 \mathbf{v}]$;
 - 6: $\mathbf{h} \leftarrow 2\mathbf{x}^{k+1} - \mathbf{x}^k$;
 - 7: $\tilde{\mathbf{u}} \leftarrow \mathbf{u}^k + \gamma_2 \mathbf{h}$;
 - 8: $\mathbf{u}^{k+1} = \tilde{\mathbf{u}} - \gamma_2 \text{prox}_{i_D} \left[\frac{1}{\gamma_2} \tilde{\mathbf{u}} \right]$;
 - 9: $\tilde{\mathbf{Y}} \leftarrow \mathbf{Y}^k + \gamma_2 [\sqrt{w_1} \mathbf{D}_1 \mathbf{h}, \dots, \sqrt{w_N} \mathbf{D}_N \mathbf{h}]$;
 - 10: $\mathbf{Y}^{k+1} = \tilde{\mathbf{Y}} - \gamma_2 \text{prox}_{\frac{\alpha}{\gamma_2} \|\cdot\|_{2,1}} \left[\frac{1}{\gamma_2} \tilde{\mathbf{Y}} \right]$;
 - 11: $\tilde{\mathcal{Z}}^{(n)} \leftarrow \mathcal{Z}^{(n)k} + \gamma_2 \mathbf{H}^{(n)}$; ($\forall n$)
 - 12: $\mathcal{Z}^{(n)k+1} = \tilde{\mathcal{Z}}^{(n)} - \gamma_2 \text{prox}_{\frac{\beta \lambda_n}{\gamma_2} \|\cdot\|_*} \left[\frac{1}{\gamma_2} \tilde{\mathcal{Z}}^{(n)} \right]$; ($\forall n$)
 - 13: $k \leftarrow k + 1$;
 - 14: **until** convergence
-

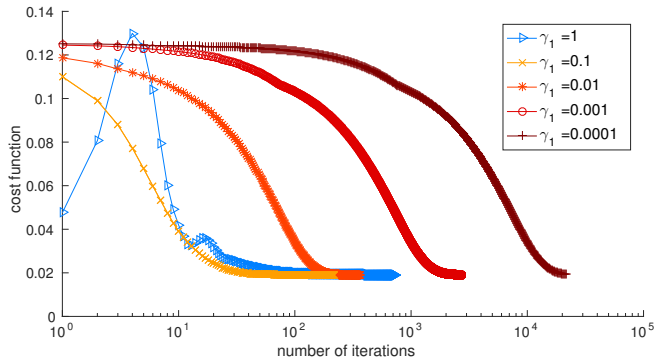


Figure 2. Convergence curves for various values of γ_1 .

where $\mathbf{z}_q, \mathbf{t}_q$, and \mathbf{x}_q are vectors consisting of all elements of \mathcal{Z}, \mathcal{T} , and \mathcal{X} , respectively, that satisfy $q_{i_1, i_2, \dots, i_N} = 1$. The solution of (24) is given by a projection of \mathbf{z}_q on the sphere with center \mathbf{t}_q and radius $\sqrt{\delta}$, or by the \mathbf{z}_q that is in that sphere. We obtain

$$\begin{aligned}
 \mathbf{x}_q^* &= \mathbf{t}_q + \min \left(\|\mathbf{z}_q - \mathbf{t}_q\|_2, \sqrt{\delta} \right) \frac{\mathbf{z}_q - \mathbf{t}_q}{\|\mathbf{z}_q - \mathbf{t}_q\|_2} \\
 &= [1 - \min(1, \eta)] \mathbf{t}_q + \min(1, \eta) \mathbf{z}_q \\
 &= \max(0, 1 - \eta) \mathbf{t}_q + [1 - \max(0, 1 - \eta)] \mathbf{z}_q, \quad (25)
 \end{aligned}$$

where $\eta = \frac{\sqrt{\delta}}{\|\mathbf{z}_q - \mathbf{t}_q\|_2}$. Eq. (21) satisfies (25). \square

5. Experiments

In this section, we compare the proposed method with several state-of-the-art methods by conducting image recovery experiments. For convex optimization, we selected LNRTC [10] and GTV [14] for comparison. In contrast, for non-convex optimization (tensor decomposition), we se-

Table 1. Values of (γ_1, γ_2)

(α, β)	(γ_1, γ_2)
(0.0, 1.0)	(1.00, 0.125)
(0.1, 0.9)	(0.50, 0.250)
(0.2, 0.8)	(0.20, 0.625)
(0.3, 0.7)	(0.10, 1.250)
(0.4, 0.6)	(0.10, 1.250)
(0.5, 0.5)	(0.05, 2.500)
(0.6, 0.4)	(0.04, 3.125)
(0.7, 0.3)	(0.03, 4.166)
(0.8, 0.2)	(0.02, 6.250)
(0.9, 0.1)	(0.01, 12.50)
(1.0, 0.0)	(0.01, 12.50)

lected smooth parallel factor (PARAFAC) tensor completion with total/quadratic variation (SPCTV/SPCQV) [32]. In contrast with LNRTC, which is based on a low Tucker-rank prior, SPCTV/SPCQV is based on a low CP-rank prior. We used the SPCTV/SPCQV MATLAB toolbox, which is distributed by IEEEEXPLORE¹. As packages for LNRTC and GTV might not be distributed, we implemented these algorithms in MATLAB. Please note that we implemented GTV using the PDS algorithm instead of the ADMM to prevent the FFT, and the solutions obtained using the ADMM and PDS should be included in the identical convex set because of the convexity of the optimization problem.

5.1. Evaluation of optimization

In this experiment, we evaluated the convergence behaviors and computational times of the proposed method. We prepared various color images in sizes of $(M [\text{pixels}] \times M [\text{pixels}] \times 3 [\text{colors}])$ for $M \in \{64, 128, 256, 512, 1024, 2048\}$; 30% voxels were arbitrarily removed and Gaussian noise was added to these images. Figure 2 shows an example of the convergence curves obtained by applying the proposed algorithm to a $(128 \times 128 \times 3)$ image with $\alpha = \beta = 0.5$ for various values of (γ_1, γ_2) , considered as $\gamma_1 \in \{0.0001, 0.001, 0.01, 0.1, 1\}$ and $\gamma_2 = 1/(8\gamma_1)$. It can be observed that the value of γ_1 should be in a suitable range to achieve convergence in a short amount of time. In practice, we determined empirically that suitable values of γ_1 depend on the values of α . For all following experiments, we selected the values of (γ_1, γ_2) based on (α, β) , by referring to Table 1, which was obtained using hand tuning. Please note that we normalized the range of values in the input tensors, \mathcal{T} , as $[0, 1]$, and considered $v_{\min} = 0$ and $v_{\max} = 1$ for optimization. This normalization is important for the selected values of γ_1, γ_2 to work correctly. For evaluation, we restore the range of values in the output tensors, \mathcal{X} , such as $[0, 255]$ for 8-bit images.

¹<http://ieeexplore.ieee.org/document/7502115/media>

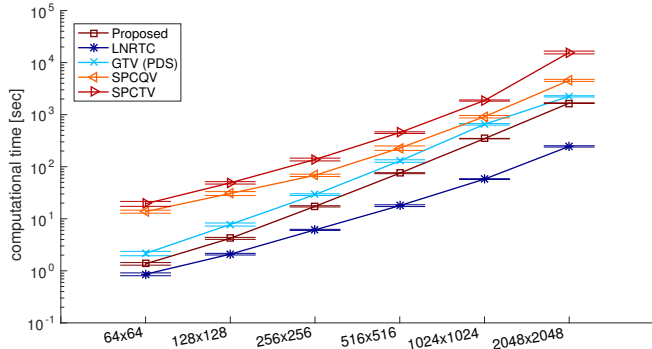


Figure 3. Computational times for various rescaled images.



Figure 4. Test color images: ‘airplane’, ‘baboon’, ‘barbara’, ‘facade’ (left to right in the first row), ‘house’, ‘lena’, ‘peppers’, ‘sailboat’ (left to right in the second row).

Figure 3 shows a comparison of the computational times of state-of-the-art tensor completion methods for various rescaled images. The lines and bars represent the averages and the standard deviations, respectively, for ten trials. It can be observed that the proposed algorithm is faster than other state-of-the-art algorithms, except LNRTC. Particularly, SPCQV and SPCTV, which are tensor decomposition based methods, were computationally expensive because they solve non-convex optimization problems. In contrast, LNRTC, GTV, and the proposed method solved convex optimization problems, and their computational times were considerably lower. LNRTC by ADMM was faster than GTV and the proposed algorithm by PDS.

5.2. Color image recovery

We evaluated the proposed method using color image completion and denoising. Figure 4 shows the test images used in this experiment. Eight images have a size of $(256 \times 256 \times 3)$. All images were corrupted by removing arbitrary voxels and adding Gaussian noise, $\mathcal{N}(0, 20)$. Missing ratios were considered as $\rho \in \{10\%, 30\%, 50\%\}$. For the proposed method, we tuned the values of α , λ , and δ to evaluate the peak signal to noise ratio (PSNR). Other parameters were considered as $\beta = 1 - \alpha$, $\mathbf{w} = [0.5, 0.5, 0.0]^T$, and $\boldsymbol{\lambda} = [\lambda/2, \lambda/2, 1 - \lambda]^T$. Figure 5 shows the color illustration of the PSNR values for various combinations of α and λ in individual images. The most suitable combinations of α and λ depend on the images. Three images, referred to as ‘house’, ‘lena’, and ‘peppers’, prefer TV regularization (large α). In contrast, ‘facade’ prefers nuclear norm regularization (small α). Other images, referred to as ‘airplane’, ‘baboon’, ‘barbara’, and ‘sailboat’, prefer intermediate mixing of TV and nuclear norm regu-

Table 3. PSNR comparison in color movie (4D tensor) completion and denoising

ρ	Proposed	GTV	LNRTC	SPCQV	SPCTV
0.1	31.045	30.947	28.820	30.018	30.021
0.3	28.942	28.485	26.920	29.642	29.659
0.5	26.750	26.101	25.006	28.995	29.996

Table 4. SDR comparison for 3D-MR image completion and denoising

name	ρ	Proposed	GTV	LNRTC	SPCQV	SPCTV
citrus	0.1	25.646	25.186	23.852	23.743	23.706
	0.3	23.410	22.920	20.948	22.251	22.115
	0.5	20.919	20.644	18.112	20.459	20.162
tomato	0.1	27.980	27.865	26.231	24.896	24.890
	0.3	27.187	26.782	24.516	24.492	24.460
	0.5	26.014	25.429	22.785	23.825	23.717

larizations.

Table 2 shows the performances of color image recovery for the proposed and selected state-of-the-art methods. For all methods, we tuned all hyperparameters to obtain the best performances manually. Except for the case of ‘facade’, the proposed method outperformed state-of-the-art methods for lower values of missing ratios (10% and 30%). The proposed method exhibited the best performance for a missing ratio of 50% for ‘house’, ‘lena’, and ‘peppers’, which prefer TV regularization, as shown in Figure 5. For ‘facade’, which prefers nuclear norm regularization, SPCTV exhibited the best performance for all missing ratios. For ‘airplane’, ‘baboon’, ‘barbara’, and ‘sailboat’, which prefer intermediate mixing, SPCQV exhibited the best performance for a missing ratio of 50%.

5.3. Color movie recovery

We evaluated the proposed method using color movie completion and denoising. A data set, referred to as ‘bootstrap’, is distributed by Microsoft Research² [29]. We corrupted it by removing arbitrary voxels and adding Gaussian noise, $\mathcal{N}(0, 10)$. The input movie (4D tensor) has a size of 120 pixels \times 160 pixels \times 3 color-channels \times 100 frames. We considered $\mathbf{w} = [0.4, 0.4, 0.0, 0.2]^T$ and $\boldsymbol{\lambda} = [0.2, 0.2, 0.2, 0.4]^T$, and (α, β, δ) were tuned manually. Figure 6 shows the results of movie recovery for the proposed and selected state-of-the-art methods with 30% missing voxels. The result for LNRTC is noisy, and the result for GTV includes minor artifacts. With respect to PSNRs, SPCTV and SPCQV were the best; however, the results were blurred. In contrast, the result for the proposed method was clear with a good PSNR. Table 3 shows the values of PSNRs for various missing ratios. The proposed method was the best for a missing ratio of 10%, and SPCTV

²<http://research.microsoft.com/en-us/um/people/jckrumm/wallflower/testimages.htm>

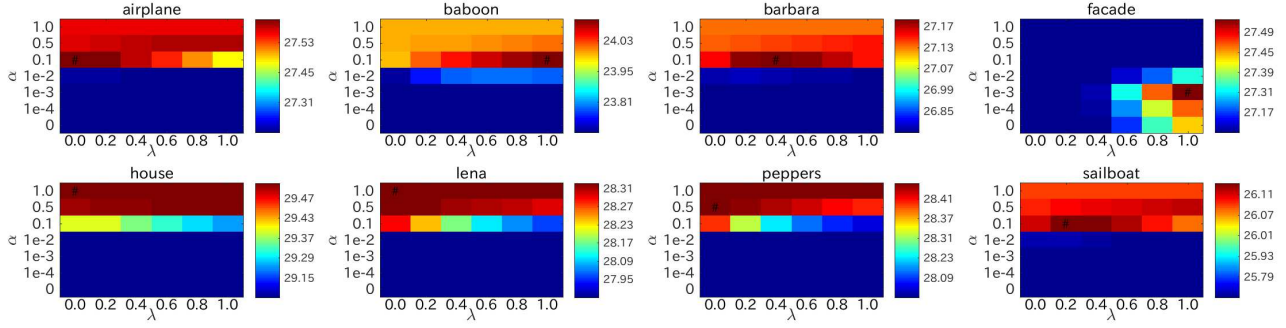


Figure 5. PSNR color maps for various values of hyperparameters α and λ using eight test color images with 30% missing elements. ‘#’ is placed on the maximum values of PSNR in each colormap.

Table 2. PSNR comparison for test color image completion and denoising

name	ρ	(α, λ)	Proposed	GTV	LNRTC	SPCQV	SPCTV
airplane	0.1	(0.100,0.200)	28.759	28.613	26.374	28.166	27.915
airplane	0.3	(0.100,0.000)	27.575	27.300	25.224	27.316	26.932
airplane	0.5	(0.100,0.200)	26.177	25.964	23.657	26.447	25.896
baboon	0.1	(0.100,1.000)	25.103	25.034	24.163	24.736	24.610
baboon	0.3	(0.100,1.000)	24.070	24.001	22.865	23.927	23.715
baboon	0.5	(0.100,1.000)	23.013	22.959	21.597	23.026	22.612
barbara	0.1	(0.100,0.800)	27.952	27.818	26.206	27.648	27.342
barbara	0.3	(0.100,0.400)	27.183	26.958	25.069	27.033	26.570
barbara	0.5	(0.100,0.200)	26.197	25.900	23.570	26.310	25.499
facade	0.1	(0.001,1.000)	28.242	25.975	27.829	28.897	28.979
facade	0.3	(0.001,1.000)	27.516	24.928	27.354	28.316	28.348
facade	0.5	(0.001,1.000)	26.555	23.672	26.300	27.431	27.469
house	0.1	(0.500,1.000)	30.329	29.962	26.885	29.037	28.633
house	0.3	(1.000,0.000)	29.501	29.106	26.100	28.452	27.923
house	0.5	(1.000,0.000)	27.975	27.780	24.519	27.592	26.929
lena	0.1	(0.500,0.000)	29.086	28.823	26.098	28.060	27.560
lena	0.3	(1.000,0.000)	28.320	27.885	25.048	27.352	26.742
lena	0.5	(0.500,0.200)	27.178	26.752	23.558	26.570	25.701
peppers	0.1	(1.000,0.000)	29.380	29.110	25.895	27.179	26.932
peppers	0.3	(0.500,0.000)	28.442	28.051	24.616	26.625	26.018
peppers	0.5	(0.500,0.000)	27.086	26.757	23.092	25.727	24.933
sailboat	0.1	(0.100,0.000)	27.386	27.162	25.374	26.487	26.316
sailboat	0.3	(0.100,0.200)	26.131	25.872	24.091	25.817	25.462
sailboat	0.5	(0.100,0.400)	24.581	24.315	22.527	24.843	24.224

was the best for missing ratios of 30% and 50%, based on PSNR comparison.

5.4. 3D-volumetric image recovery

We evaluated the proposed method using completion and denoising for 3D-volumetric magnetic resonance (MR) images. Figure 7 shows test MR images and examples of corrupted and recovered images. MR images were obtained using a micro-MR imaging system. Original MR images include minor noise. However, we assumed these images as ground truth images, and corrupted these images synthetically for evaluation. Two MR images referred to as ‘citrus’ and ‘tomato’ have a size of $(256 \times 256 \times 24)$. As each

voxel value is obtained using integration of a $(1.5/8 \text{ mm} \times 1.5/8 \text{ mm} \times 1.5 \text{ mm})$ -volume, the resolutions of the (x,y,z) -axes are anisotropic. We consider $w = [8/17, 8/17, 1/17]^T$ and $\lambda = [1/3, 1/3, 1/3]^T$, and (α, β, δ) are tuned manually. Table 4 shows the signal-to-distortion ratio (SDR) obtained using the proposed and state-of-the-art methods for MR image completion and denoising. It can be observed that the proposed method outperforms all state-of-the-art methods for all missing ratios.

6. Conclusions

In this paper, we proposed a new model and algorithm for simultaneous tensor completion and denoising based

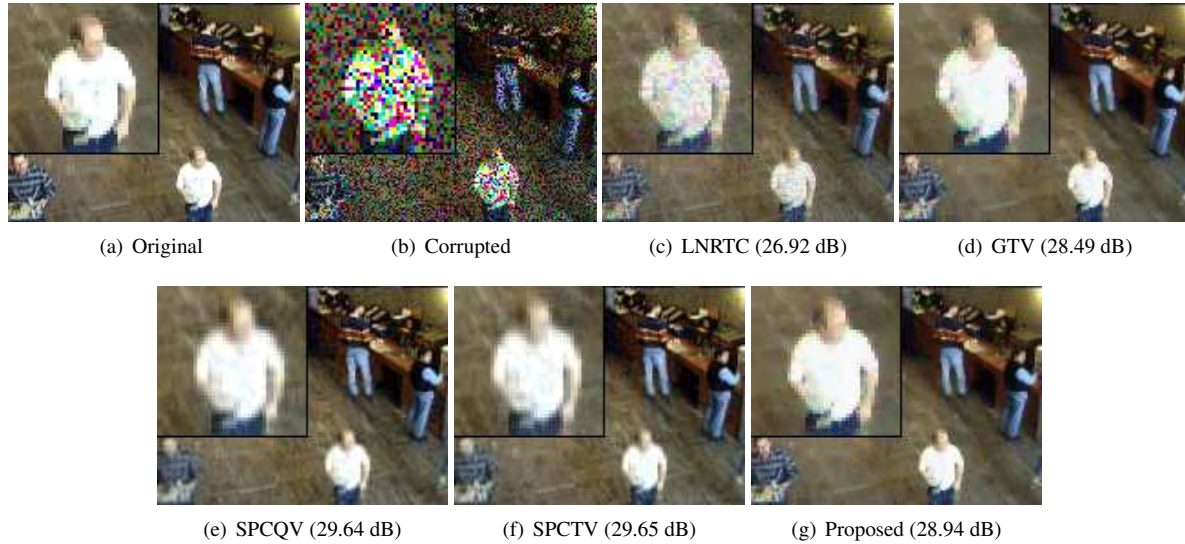


Figure 6. Experimental results of color movie (4D tensor) completion and denoising: original data has a size of $(120 \times 160 \times 3 \times 100)$ and is corrupted by 30% missing voxels and Gaussian noise ($\sigma = 10$). The 5th frame image, PSNRs, and computational times are described for all methods.

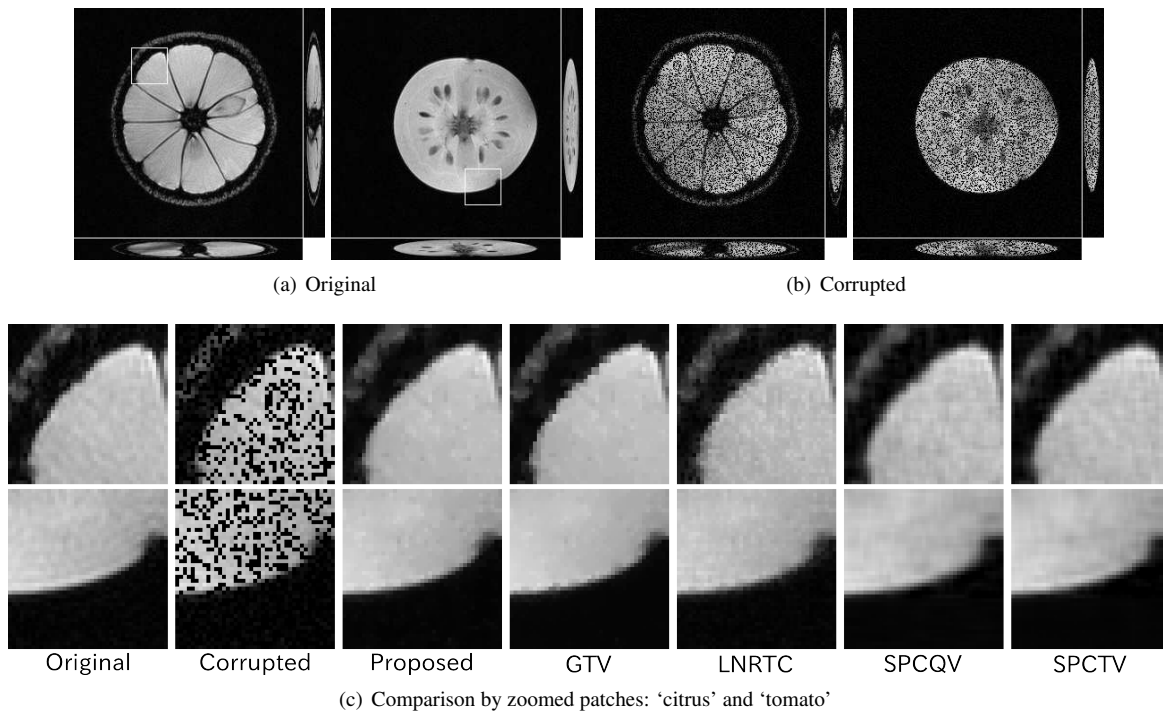


Figure 7. Test 3D-MR image in a size of $256 \times 256 \times 24$: (a) original full-observed image: 'citrus' (left) and 'tomato' (right), (b) image with 30% missing elements corrupted by Gaussian noise, (c) patches of recovered images using the proposed and selected state-of-the-art methods.

on nuclear norms and TV minimization. The proposed model can be characterized as a generalization of several prior works. Extensive experiments demonstrated that the proposed method outperformed various state-of-the-art tensor completion methods for color images, movies, and 3D-

volumetric data retrieval.

Acknowledgement

This work was supported by Japan Society for the Promotion of Science KAKENHI Grant Number 15K16067.

References

- [1] D. P. Bertsekas. *Convex Optimization Algorithms*. Athena Scientific, 2015. [2](#)
- [2] S. Boyd, N. Parikh, E. Chu, B. Peleato, and J. Eckstein. Distributed optimization and statistical learning via the alternating direction method of multipliers. *Foundations and Trends® in Machine Learning*, 3(1):1–122, 2011. [3](#)
- [3] J. F. Cai, E. J. Candes, and Z. Shen. A singular value thresholding algorithm for matrix completion. *SIAM Journal on Optimization*, 20(4):1956–1982, 2010. [1](#)
- [4] E. J. Candès, X. Li, Y. Ma, and J. Wright. Robust principal component analysis? *Journal of the ACM (JACM)*, 58(3):11, 2011. [1](#)
- [5] E. J. Candes and Y. Plan. Matrix completion with noise. *Proceedings of the IEEE*, 98(6):925–936, 2010. [1](#), [2](#), [3](#)
- [6] E. J. Candes and B. Recht. Exact matrix completion via convex optimization. *Foundations of Computational Mathematics*, 9(6):717–772, 2009. [1](#)
- [7] E. J. Candes and T. Tao. The power of convex relaxation: Near-optimal matrix completion. *IEEE Transactions on Information Theory*, 56(5):2053–2080, 2010. [1](#)
- [8] C. Chen, B. He, and X. Yuan. Matrix completion via an alternating direction method. *IMA Journal of Numerical Analysis*, 32(1):227–245, 2012. [1](#)
- [9] L. Condat. A primal–dual splitting method for convex optimization involving Lipschitzian, proximable and linear composite terms. *Journal of Optimization Theory and Applications*, 158(2):460–479, 2013. [1](#), [2](#), [4](#)
- [10] S. Gandy, B. Recht, and I. Yamada. Tensor completion and low-n-rank tensor recovery via convex optimization. *Inverse Problems*, 27(2), 2011. [3](#), [5](#)
- [11] N. Gillis and F. Glineur. Low-rank matrix approximation with weights or missing data is NP-hard. *SIAM Journal on Matrix Analysis and Applications*, 32(4):1149–1165, 2011. [1](#)
- [12] N. Gillis and S. A. Vavasis. Fast and robust recursive algorithms for separable nonnegative matrix factorization. *IEEE Transactions on Pattern Analysis and Machine Intelligence*, 36(4):698–714, 2014. [1](#)
- [13] F. Guichard and F. Malgouyres. Total variation based interpolation. In *Signal Processing Conference (EUSIPCO 1998)*, 9th European, pages 1–4. IEEE, 1998. [2](#)
- [14] X. Guo and Y. Ma. Generalized tensor total variation minimization for visual data recovery. In *2015 IEEE Conference on Computer Vision and Pattern Recognition (CVPR)*, pages 3603–3611, 2015. [3](#), [5](#)
- [15] H. Ji, C. Liu, Z. Shen, and Y. Xu. Robust video denoising using low rank matrix completion. In *Proceedings of IEEE Conference on Computer Vision and Pattern Recognition (CVPR)*, pages 1791–1798. IEEE, 2010. [1](#)
- [16] T.-Y. Ji, T.-Z. Huang, X.-L. Zhao, T.-H. Ma, and G. Liu. Tensor completion using total variation and low-rank matrix factorization. *Information Sciences*, 326:243–257, 2016. [4](#)
- [17] R. H. Keshavan, A. Montanari, and S. Oh. Matrix completion from noisy entries. In *Advances in Neural Information Processing Systems*, pages 952–960, 2009. [1](#)
- [18] R. H. Keshavan, A. Montanari, and S. Oh. Matrix completion from a few entries. *IEEE Transactions on Information Theory*, 56(6):2980–2998, 2010. [1](#)
- [19] T. G. Kolda and B. W. Bader. Tensor decompositions and applications. *SIAM review*, 51(3):455–500, 2009. [3](#)
- [20] D. Kressner, M. Steinlechner, and B. Vandereycken. Low-rank tensor completion by Riemannian optimization. *BIT Numerical Mathematics*, 54(2):447–468, 2014. [1](#)
- [21] G. Liu, Z. Lin, and Y. Yu. Robust subspace segmentation by low-rank representation. In *Proceedings of the 27th International Conference on Machine Learning (ICML-10)*, pages 663–670, 2010. [1](#)
- [22] J. Liu, P. Musialski, P. Wonka, and J. Ye. Tensor completion for estimating missing values in visual data. In *Proceedings of International Conference on Computer Vision (ICCV)*, pages 2114–2121. IEEE, 2009. [3](#)
- [23] J. Liu, P. Musialski, P. Wonka, and J. Ye. Tensor completion for estimating missing values in visual data. *IEEE Transactions on Pattern Analysis and Machine Intelligence*, 35(1):208–220, 2013. [1](#), [3](#)
- [24] S. Ma, D. Goldfarb, and L. Chen. Fixed point and Bregman iterative methods for matrix rank minimization. *Mathematical Programming*, 128(1-2):321–353, 2011. [1](#), [2](#)
- [25] L. Miao and H. Qi. Endmember extraction from highly mixed data using minimum volume constrained nonnegative matrix factorization. *IEEE Transactions on Geoscience and Remote Sensing*, 45(3):765–777, 2007. [1](#)
- [26] B. Recht, M. Fazel, and P. A. Parrilo. Guaranteed minimum-rank solutions of linear matrix equations via nuclear norm minimization. *SIAM Review*, 52(3):471–501, 2010. [1](#)
- [27] L. I. Rudin, S. Osher, and E. Fatemi. Nonlinear total variation based noise removal algorithms. *Physica D: Nonlinear Phenomena*, 60(1):259–268, 1992. [2](#)
- [28] F. Shi, J. Cheng, L. Wang, P.-T. Yap, and D. Shen. Low-rank total variation for image super-resolution. In *International Conference on Medical Image Computing and Computer-Assisted Intervention*, pages 155–162. Springer, 2013. [2](#)
- [29] K. Toyama, J. Krumm, B. Brumitt, and B. Meyers. Wallflower: Principles and practice of background maintenance. In *Seventh International Conference on Computer Vision*, pages 255–261, 1999. [6](#)
- [30] C. R. Vogel and M. E. Oman. Fast, robust total variation-based reconstruction of noisy, blurred images. *IEEE Transactions on Image Processing*, 7(6):813–824, 1998. [2](#)
- [31] G. K. Wallace. The JPEG still picture compression standard. *IEEE Transactions on Consumer Electronics*, 38(1):xviii–xxxiv, 1992. [1](#)
- [32] T. Yokota, Q. Zhao, and A. Cichocki. Smooth PARAFAC decomposition for tensor completion. *IEEE Transactions on Signal Processing*, 64(20):5423–5436, 2016. [5](#)